Strong attenuation of high water levels observed in tropical mangroves

Pelckmans, Ignace; Vermeulen, Ben; Ramos-Veliz, John Alex; Rosado-Moncayo, Andrea Mishell; Belliard, Jean Philippe; Gourgue, Olivier; Slobbe, Cornelis; Dominguez-Granda, Luis E.; Temmerman, Stijn

DOI
10.1002/lno.70131

Publication date
2025

Document Version
Final published version

Published in
Limnology and Oceanography

Citation (APA)
Pelckmans, I., Vermeulen, B., Ramos-Veliz, J. A., Rosado-Moncayo, A. M., Belliard, J. P., Gourgue, O., Slobbe, C., Dominguez-Granda, L. E., & Temmerman, S. (2025). Strong attenuation of high water levels observed in tropical mangroves. *Limnology and Oceanography*, *70*(9), 2405-2416. https://doi.org/10.1002/lno.70131

LIMNOLOGY and OCEANOGRAPHY

ASLO

Limnol. Oceanogr. 70, 2025, 2405–2416

doi: 10.1002/lno.70131

RESEARCH ARTICLE

Strong attenuation of high water levels observed in tropical mangroves

Ignace Pelckmans,[1*] **Ben Vermeulen**,[1] **John Alex Ramos-Veliz**,[2] **Andrea Mishell Rosado-Moncayo**,[2] **Jean-Philippe Belliard**,[1,3] **Olivier Gourgue**,[3] **Cornelis Slobbe**,[4] **Luis E. Dominguez-Granda**,[2] **Stijn Temmerman**[1]

[1]ECOSPHERE Research Group, University of Antwerp, Antwerp, Belgium; [2]Centro del Agua y Desarrollo Sostenible, Facultad de Ciencias Naturales y Matemáticas, Escuela Superior Politécnica del Litoral (ESPOL), Guayaquil, Ecuador; [3]Operational Directorate Natural Environment, Royal Belgian Institute of Natural Sciences, Brussels, Belgium; [4]Delft Institute of Earth Observation and Space Systems, Delft University of Technology, Delft, The Netherlands

Abstract

Mangroves are more and more recognized for nature-based mitigation of flood risks in low-lying coastal zones, which host a disproportionately large part of the global population. Aerial roots, branches, and canopy of mangrove trees exert friction on the water flow, thereby reducing the propagation of high water levels through the forest. Field measurements of high water level attenuation rates are limited so far to mangrove forests situated at higher-latitude subtropical settings, where aerial roots are much sparser and lower than in low-latitude tropical mangroves. Here, for the first time, we measured high water level attenuation in a tropical *Rhizophora* forest, where aerial roots are several meters high and water levels never exceeded the aerial root height. Our measurements reveal attenuation rates between 42 ± 9.8 and 46 ± 9.8 cm km^{-1}, which are the highest attenuation rates ever recorded in a mangrove forest, but an exponential rate is more suited to quantify high water level attenuation. In contrast to observations inside the mangrove forest, our observations showed that the propagation of high water levels through a 20 km long tidal channel fringed by wide mangrove areas was amplified, but that high water level amplification was reduced for higher tides with deeper flooding of the fringing mangroves. Our results provide the first empirical assessment of flood protection by tropical *Rhizophora* mangroves. As *Rhizophora* is globally the most common genus among mangroves, we propose that our reported high attenuation rates should be incorporated in future assessments of nature-based flood risk mitigation by mangroves.

Low-lying coasts host a disproportionately large part of the global population but are increasingly threatened by sea-born flood risks driven by processes such as storm surges, tsunamis and extreme high tides (Fox-Kemper et al. 2021; Tebaldi et al. 2021; Glavovic et al. 2022). By 2050, such extreme sea level events are expected to occur 20–30 times more frequently than in the recent past (Fox-Kemper et al. 2021) due to global mean sea level rise, increasing storm intensity in some regions, and local land subsidence. To mitigate these risks in the (sub)tropics, mangrove conservation and restoration are more and more recognized as nature-based solutions for coastal protection (Glass et al. 2018; Gijsman et al. 2021; Temmerman et al. 2023).

Empirical studies have shown that mangroves can reduce storm and tsunami impacts by lowering economic loss and casualties (Das and Vincent 2009; Dahdouh-Guebas et al. 2005; Kathiresan and Rajendran 2005; del Valle et al. 2020), while modeling studies have further extended on the landward reduction of extreme sea levels (Zhang et al. 2012; Deb and Ferreira 2017; Chen et al. 2021; Pelckmans et al. 2024). Yet, field measurements of high water level (HWL) attenuation within and behind mangrove forests remain very scarce with, to our knowledge, only three reports of measured attenuation rates in the scientific literature (Table 1), hence limiting empirical insights and the capacity to calibrate and validate

*Correspondence: ignace.pelckmans@uantwerpen.be

Associate editor: Ruth Reef

Data Availability Statement: The data that support the findings of this study are openly available in Zenodo at [https://doi.org/10.5281/zenodo.15434117].

predictive models against data. Attenuation is typically expressed as vertical reduction in HWL per horizontal distance traveled by the tide or surge (cm km^{-1}). We can distinguish two types of attenuation. First, when HWLs propagate through continuous mangroves, the branches, aerial roots, and canopy of mangroves exert friction on the water flow, thereby reducing peak water levels when propagating (Mazda et al. 1997). This is referred to as *within-wetland attenuation* (Temmerman et al. 2023). In a coastal wetland zone with mixed mangrove and marsh vegetation in Florida, Krauss et al. (2009) measured HWL reduction of 9.5 cm km^{-1}. In continuous subtropical mangroves in New Zealand, dominated by *Avicennia marina*, measured attenuation rates were 24 cm km^{-1} (Montgomery et al. 2018) and 36 cm km^{-1} (Horstman et al. 2021). Second, mangroves are often dissected by tidal channels, which facilitate the propagation of tides and surges, as compared to the surrounding higher-elevated, densely vegetated mangroves. When rising water levels exceed the channel banks, the water spreads out into the mangroves, thereby reducing upstream water levels in the channels (Horstman et al. 2013; Smolders et al. 2015). This is referred to as *along-channel* attenuation, and typically presents much smaller attenuation rates than *within-wetland* attenuation, with values ranging between 0 and 12 cm km^{-1} (Krauss et al. 2009; Montgomery et al. 2018; Horstman et al. 2021).

The few existing studies are limited to specific mangrove settings that are not representative of the global extent of mangroves, that is, they are limited to (1) mangroves dominated by *Avicennia marina* (Table 1) and (2) mangroves (or mangrove-marsh mixtures) at higher latitudes close to their most northern or southern ranges. In *Avicennia marina* mangrove forests, the vegetation-induced drag is mainly caused by a dense network of pneumatophores, typically less than 30 cm high (Chen 2016; Montgomery et al. 2018; Horstman et al. 2021) (Supporting Information Fig. S2). Besides *Avicennia*, *Rhizophora* species are considered one of the most commonly found mangrove species globally (Ong et al. 2004; Pil et al. 2011; Sandoval-Castro et al. 2012; Record et al. 2013; Twomey and Lovelock 2024). *Rhizophora* species are characterized by a typical complex network of above-ground stilt roots, which commonly extends one to several meters above the soil surface and therefore likely exhibits the highest drag on extreme water level propagation among mangrove species (Figs. 1, 2c; Supporting Information Fig. S2) (Krauss et al. 2003; Horstman et al. 2014). However, no studies have reported attenuation rates over large areas of natural *Rhizophora*-dominated mangroves, despite their global distribution, nor are there published observations of attenuation measurements in tropical, near-equatorial mangroves. Near-equatorial mangroves can reach canopy heights up to three times taller than those at higher latitudes (Simard 2019), with stilt root density and height increasing accordingly, enhancing drag on water flow (Mori et al. 2022). Thus, published attenuation rates may underestimate high-water-level attenuation in tropical Rhizophora-dominated mangroves.

Hence, as summarized above, currently reported observations of HWL attenuation rates in mangroves, and how they depend on within-wetland vs. along-channel attenuation mechanisms, are limited to higher latitude subtropical settings, where attenuation rates are expected to be on the lower hand. To complement the limited empirical record, we measured HWLs per tidal wave in a tropical, near-equatorial *Rhizophora*-dominated estuary in Ecuador for which we report the observed HWL attenuation rates. Since aerial roots reach several meters above the ground, water did not exceed the aerial roots. Furthermore, we compare within-wetland attenuation rates with along-channel attenuation rates on the forest scale, that is, along a 20-km channel transect completely fringed by large mangrove areas. As such, our study reports the highest HWL attenuation rates ever documented in mangroves, and it suggests potential trade-offs between within-wetland and along-channel attenuation rates.

Methods

Study area

The observed high water attenuation rates in this paper were measured in the Churute subestuary in Ecuador (Fig. 2a) which covers ± 20,000 ha and is located inside a protected nature reserve (i.e., *Reserva Ecológica Manglares Churute*). The estuary is drained by a tidal channel network which is ± 2 km wide at its, branching inland into smaller creeks. These

Table 1. Overview of published studies that include measured HWL attenuation rates.

Author	Within wetland attenuation	Along-channel attenuation and transect length	Vegetation	Country
Krauss et al. 2009	3.2–9.4 cm km^{-1}	4.2 cm km^{-1} 14.1 km	Mangrove-marsh complex	Florida
Montgomery et al. 2018	24 cm km^{-1} 800 m	± 0 cm km^{-1} 1100 m	*Avicennia marina*	New Zealand
Horstman et al. 2021	36 cm km^{-1} ± 500 m	12 cm km^{-1} ± 500 m	*Avicennia marina*	New Zealand

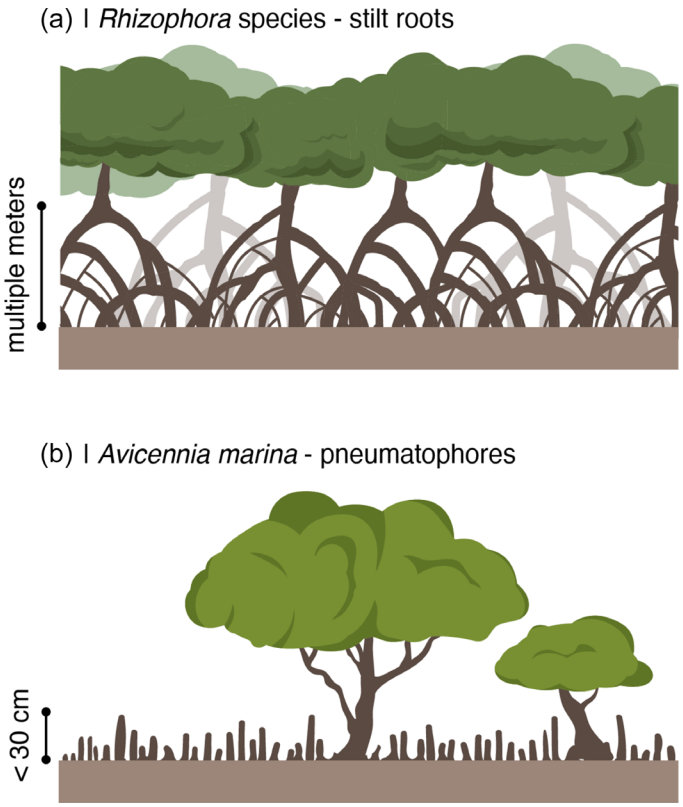

Fig. 1. Illustration of *Rhizophora* species (**a**) with their associated stilt roots, which can reach multiple meters above the mangrove forest floor, and of *Avicennia marina* mangroves (**b**) with the associated pneumatophores, which typically reach less than 30 cm above the mangrove forest floor.

channels dissect a continuous mangrove forest, dominated by *Rhizophora mangle* (Fig. 2c), which on the reserve's landward boundaries is bordered landward by leveed aquaculture ponds. The basin is fed by freshwater draining from the 300 km^2 catchment of the *Rio Churute*. While discharge measurements for this catchment are lacking, river discharge in the region is subjected to a dry season (April–November) and a wet season (December–March), with discharges varying up to eightfold (INAMHI 2019). The Churute basin lies within Guayas delta, which is a large river delta entering from the Gulf of Guayaquil (Fig. 2b). Tidal range at the delta's mouth is ~ 2 m, increasing to ~ 4 m upstream at the entrance of the Churute subestuary.

Water level loggers

We deployed 11 water level loggers (Rugged Troll 100, In-Situ) during a spring neap cycle during the dry season between August and October 2022 in the main channel and in the mangroves. Four loggers (M1–M4) were deployed at 45, 100, 220, and 400 m euclidean distance from the channel inside the mangrove forest approximately 3 cm above the forest floor. Since there are no small channels near the transect (< 1 km), we assume that the tidal flow path is perpendicular to the mangrove forest edge (Kobashi and Mazda 2005). Seven loggers (C1–7) were deployed along a 20 km transect following one of the main creeks of the Churute basin (Fig. 2a). All loggers were installed on the creek banks between the minimum and maximum HWL during spring tides (Supporting Information Fig. S3b).

Logger elevation and vertical reference

For all loggers, we measured the elevation to calculate water levels from the measured water depths. For the loggers in the mangrove forest (M1–M4) we measured the elevation, relative to water level sensor C1 (Fig. 2a), by means of trigonometric leveling (using a Sokkia SET-510 K total station) (Supporting Information Fig. S3a). More information on the procedure is given in Supporting Information Section S3.

Due to the large distances between loggers, elevation could not be surveyed with a total station. Instead, we used a differential GPS (Trimble R8s) within 25 m of each logger, placing it on rigid, canopy-free mangrove trunks or branches at the forest–channel edge (Supporting Information Fig. S3b). GPS deployment spanned at least 1 h, which allowed obtaining cm-accurate coordinates through post-processing kinematic adjustment. We measured the elevation difference between the GPS location and the logger with trigonometric leveling using a total station. The resulting water levels are referenced to the WGS84 ellipsoid. The vertical uncertainty on these ellipsoidal water levels is the sum of estimated GPS error and the trigonometric leveling uncertainty, summed with water level logger error, ultimately ranging between ± 2.4 and ± 5.1 cm (Supporting Information Table S4).

The water levels observed at C1–7 will be referenced to the geoid. The geoid is a level or equipotential surface of Earth's gravity field that represents the true horizontal. As gravity only acts in the vertical direction, a geoid is well suited as a vertical reference level to compare absolute water levels in between locations (Slobbe et al. 2013). Here, we reference all water levels to GEOID2021, being the most recent regional geoid for Ecuador (de Matos et al. 2021) and refer to these water levels as HWL_{G2021}. However, the geoid adds a source of uncertainty which for GEOID2021 can be as high as 0.92 m in terms of the root mean square error. Nevertheless, over short distances geoid height errors are typically strongly correlated (e.g., Klees and Slobbe 2023) and as such, will cancel out when comparing water levels between loggers and we can ignore this contribution to the overall uncertainty budget of the measured water levels and attenuation rates. Alternatively, we present water levels relative to a local neap tide HWL. For each logger, the HWL on September 19, 2022 (a neap tide), was subtracted from all measured HWLs. Thus, the highest water level during that tide is defined as 0 cm above the local neap tide (HWL_{NEAP}). HWLs recorded by sensors inside the mangroves (M1–M4) are referenced to an equipotential surface

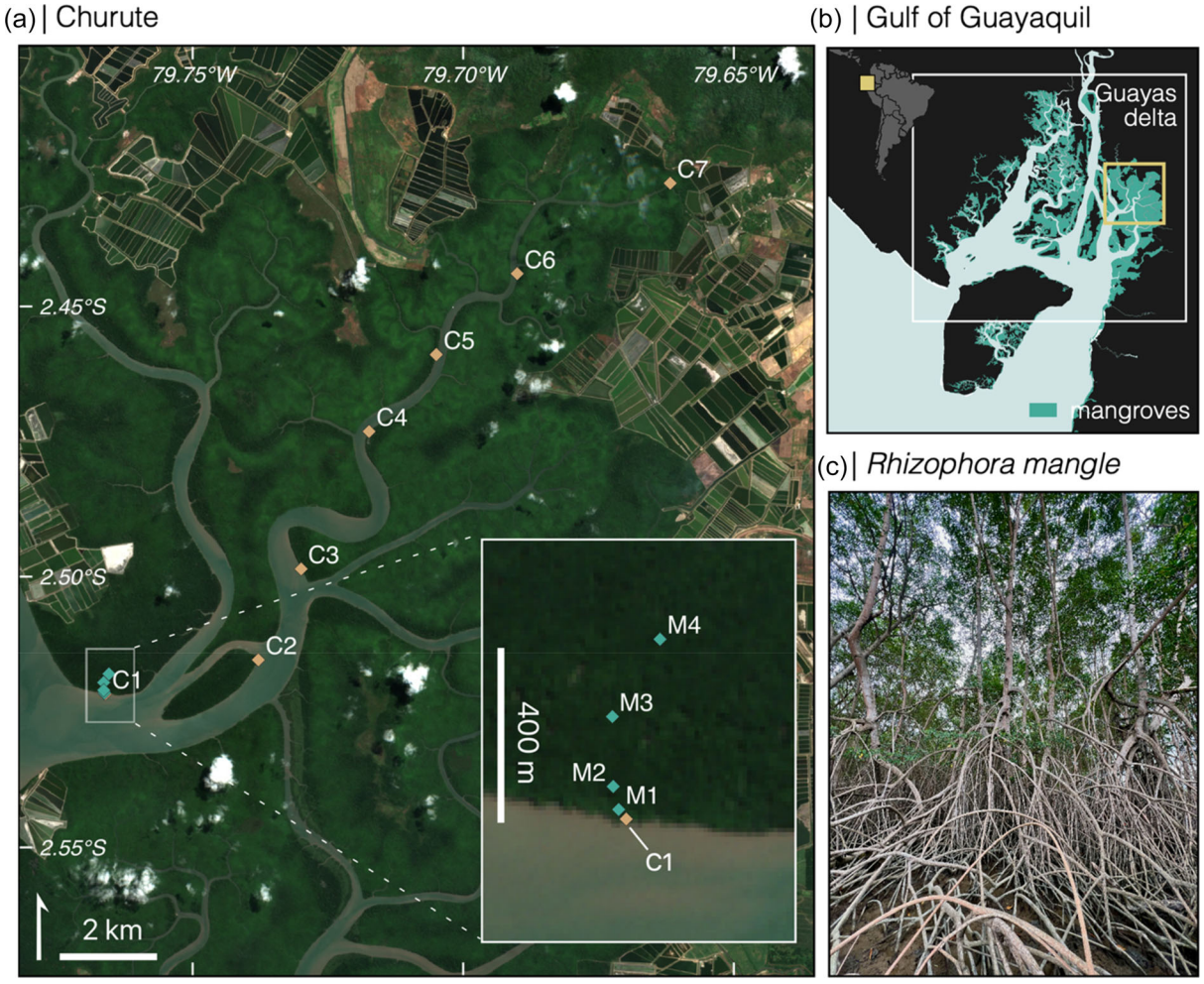

Fig. 2. Map showing the Churute study area (**a**) with the location of the water level loggers placed on the channel banks (yellow markers) and water level loggers in the mangrove forest (green markers). The study area (yellow rectangle) located in a protected area largely covered by mangroves in the east of the Guayas delta (white rectangle), located in the Gulf of Guayaquil along the coast of Ecuador (**b**). Churute is predominantly covered by Rhizophora mangle and its typical stilt roots (**c**).

aligned with the zero level of logger C1, using elevation differences measured via a leveled total station.

Calculation of attenuation rates

For each tidal cycle that was surveyed, we extracted the HWL per tidal wave from all loggers. Within-wetland attenuation rates are calculated as the landward increase or decrease in HWL between M4 (inside the forest) and C1 (at the forest edge) divided by the euclidean distance between M4 and C1. Along-channel attenuation rates are calculated as the upstream increase or decrease in HWL between C1 and C7 divided by the pathway length following the channel between C1 and C7. Both within-wetland and along-channel attenuation rates are referred to as ΔHWL rates. If HWLs increase in a landward direction, ΔHWL rates are positive and HWLs are amplified. If HWLs decrease in a landward direction, ΔHWL rates are negative and HWLs are attenuated. Errors on ΔHWL rates are calculated as the sum of the water level errors for the two associated loggers, divided by the distance in between them, those being the Euclidean distance for sensors M1–M4 and pathway length along the channel for sensors C1–C7. Not all loggers were deployed over the exact same period, but 47 HWLs were captured by all loggers in the creek and 8 HWLs were captured by all mangrove loggers (coverage periods are shown in Supporting Information Fig. S5). Along-channel rates can be calculated on HWLs referenced to both the GEOID2021 geoid or neap tide, and therefore the used reference level is indicated in subscript.

HWLs do not necessarily decrease linearly with distance (Montgomery et al. 2018), as may be suggested by the common use of attenuation rates in cm km^{-1}. Therefore, we also describe within-wetland attenuation as an exponential decay, similar to the quantification of wind wave attenuation by Zhang et al. (2022):

$$K = \frac{-\log\left(\frac{HWL_X}{HWL_0}\right)}{X} \quad (1)$$

$$HWL_x = (HWL_0 - b^*) \times e^{-Kx} + b^* \quad (2)$$

where K is the decay or exponential attenuation rate (km^{-1}), HWL_X is the high water level (cm) at a distance X from the forest edge (m) for which we considered the HWL at 400 m, HWL_0 is the high water level (cm) at the forest edge (0) and b* is a constant forest floor elevation which was set equal to 235 cm (representative forest floor elevation; Fig. 3).

Numerical model to estimate mangrove-induced drag

Previous studies on within-wetland attenuation in mangrove forests have estimated vegetation-induced drag using measurements of above-ground root structures, stem diameters, and stem densities (Montgomery et al. 2018; Horstman et al. 2021). These parameters allow for the calculation of frontal area (a_v), defined as the surface area in the vertical plane perpendicular to water flow (Zhang et al. 2015; Yoshikai et al. 2022). Vegetation-induced drag scales linearly with frontal area and the element drag coefficient (C_d), which quantifies the drag exerted by a single mangrove root or stem. This can be represented by a bulk drag coefficient for mangroves (Mazda et al. 1997; Pelckmans et al. 2023).

$$C_m = C_d \times a_v \quad (3)$$

In our study area, the complex structure of Rhizophora stilt roots made it impractical to directly measure frontal area. Instead, we estimated C_m using a numerical hydrodynamic model (TELEMAC 2D) to simulate HWL propagation through a continuous mangrove forest within a 200 m × 1000 m rectangular domain. The open boundary condition was defined using water level data from station C1, and simulations were run for all tidal events with available observational data (T1–T4). For each event, C_m was calibrated to align modeled water levels with observed data. Further details on the model setup are provided in Supporting Information Section S6.

Results

Within-wetland attenuation

In the mangrove forest, all HWLs decrease when propagating deeper into the forest (Fig. 3a) between 17 and 19 cm over 400 m (Fig. 3b), corresponding to negative ΔHWL rates of -46.2 ± 9.8 and -42.7 ± 9.8 cm km^{-1}, meaning HWL attenuation (Fig. 4). In the first 100 m, there is no clear increase or decrease. Between 100 and 220 m, the decrease is the strongest before slightly weakening between 220 and 400 m, indicating an exponential decrease of HWL with distance into the forest. In the mangrove forest, there is no significant linear relation ($R^2 = 0.096$ and p value of slope coefficient = 0.417) between ΔHWL rates and incoming HWL at the edge of the forest (Fig. 4).

When high-water level (HWL) attenuation in the mangrove forest is quantified using an exponential decay function, the

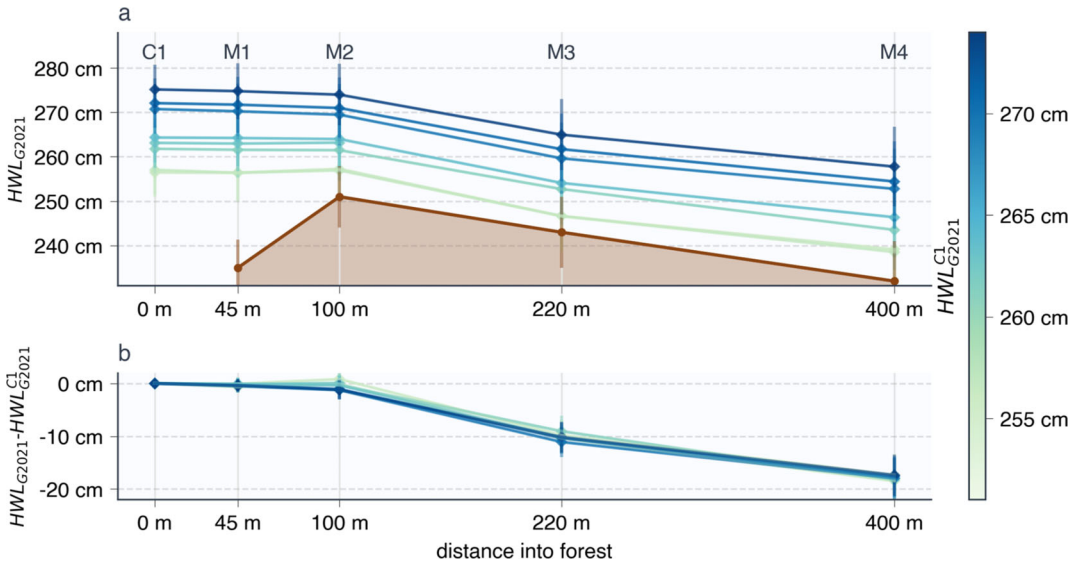

Fig. 3. High water levels referenced to GEOID2021 (**a**) and the difference between high water level along the channel and high water level in C1 (**b**) at five locations with increasing distance into the forest. Each line represents a single high tide, exceeding the channel banks, between September 10, 2022 and September 15, 2022. Darker blue colors indicate higher incoming water levels at C1, while light green colors indicate lower incoming water levels at C1 with water levels referenced to GEOD2021 ($n = 7$). The brown line and shade in (**a**) indicate the estimated mangrove forest floor elevation (height of logger minus 3 cm).

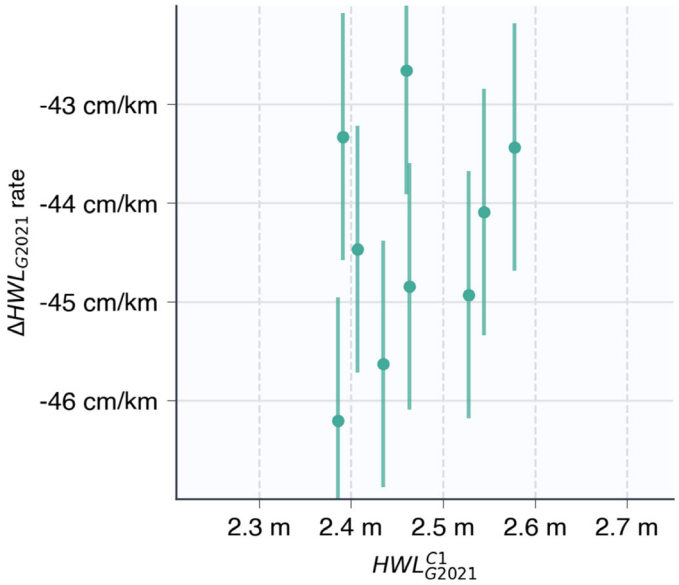

Fig. 4. ΔHWL rates inside the mangrove forest, plotted against incoming water level at C1. ΔHWL rates are calculated as the difference in peak water level for each high tide at C1 and M4 divided by the distance in between ($n = 9$). Error bars represent uncertainty between attenuation rates of different tidal waves (coming from logger uncertainty). Total uncertainties on ΔHWL rates are 9.8 cm km^{-1} for each tidal wave.

decay rate (K) tends to decrease as the inundation depth at the forest edge increases (Table 2). The observed K values range from 1.42 to 4.12 km^{-1}. Notably, for the highest tidal events and at distances greater than 400 m into the forest, the exponential model more accurately captures within-wetland attenuation than a simple linear approximation in cm km^{-1} (Supporting Information Fig. S7). Estimated values of the mangrove-induced drag coefficient (C_m) range between 1 and 3 (Table 2) with generally lower values for C_m for tides with higher inundation depth. Simulated within-wetland attenuation increases with higher C_m values. Further details on the method for estimating C_m are provided in Supporting Information Section S6.

Along-channel amplification

Along the 20-km channel transect, absolute HWLs consistently increase upstream during all recorded high tides, though the rate of increase diminishes with higher incoming water levels and varies across transect sections (Fig. 5a). Overall, HWL increases range from 14 to 21 cm, corresponding to ΔHWL rates of + 0.7 to + 1.1 cm km^{-1}, indicating amplification. In the first 6 km, HWLs rise by 8–11 cm (ΔHWL: + 1.3 to + 1.8 cm km^{-1}). Between 6 and 13 km, HWLs decrease by up to 8 cm or remain nearly stable (ΔHWL: − 1.3 to + 0.1 cm km^{-1}), while in the final 7 km, they increase again by 17–24 cm (ΔHWL: + 2.5 to + 3.4 cm km^{-1}). When considering the HWLs relative to the local neap tide HWL, they also increase but with a lower increase between 0 and 8 cm. In the first 13 km, HWLs rise under lower incoming tides (< 80 cm) but decline under higher ones (> 80 cm; Fig. 5b). In contrast, HWLs in the final 7 km increase regardless of incoming tide height.

ΔHWL rates across the transect increase with incoming HWL up to 0.5 m above the neap tide level (2.1 m relative to GEOID2021), after which they decline (Fig. 6). Rates shown in Fig. 6 are based on measurements between loggers C1 and C6, which recorded the most HWLs ($n = 98$). Relative to GEOID2021, ΔHWL ranges from + 0.3 to + 0.7 cm km^{-1} (amplification), and from − 0.2 to + 0.3 cm km^{-1} relative to the neap tide. For incoming levels above 0.54 m (neap tide reference), ΔHWL decreases linearly with water level ($R^2 = 0.89$). Below this threshold, a weaker positive linear trend is observed ($R^2 = 0.39$).

Discussion

Nature-based solutions for sea-born flood risk mitigation are receiving much attention in scientific literature (Glass et al. 2018; Gijsman et al. 2021; Temmerman et al. 2023). Yet, direct measurements of HWL attenuation within mangrove forests are very scarce and limited to mangrove-marsh mixtures or *Avicennia* mangroves near their most northern or southern ranges. Here we present measured ΔHWL rates, for the first time inside a near-equatorial *Rhizophora* dominated mangrove forest, ranging between − 42.7 ± 9.8 and − 46.2 ± 9.8 cm km^{-1}, which are by far the strongest HWL attenuation rates ever measured within mangroves. However, along a 20-km long estuarine channel that is dissecting the *Rhizophora* mangrove forest, we observed positive ΔHWL rates, meaning HWLs are not attenuated but amplified, which is likely due to the funnel-shaped geometry of the channel.

Within-wetland attenuation

We have measured within-wetland ΔHWL rates between − 42 ± 9.8 cm km^{-1} and − 46 ± 9.8 cm km^{-1} (Fig. 4) while previous studies measured between − 3.2 cm km^{-1} and − 36 cm km^{-1} (Table 1). We attribute our high values to the

Table 2. Calculated exponential attenuation rates (km^{-1}, *see* Eq. 1) and estimated values for C_m based on numerical model calibration for seven recorded tidal waves with varying inundation depth at the forest edge.

Inundation at forest edge	21 cm	22 cm	27 cm	29 cm	36 cm	37 cm	40 cm
K	4.12	4.56	2.86	2.37	1.75	1.62	1.42
C_m	2.5	3	1.5	1.5	1	1	1

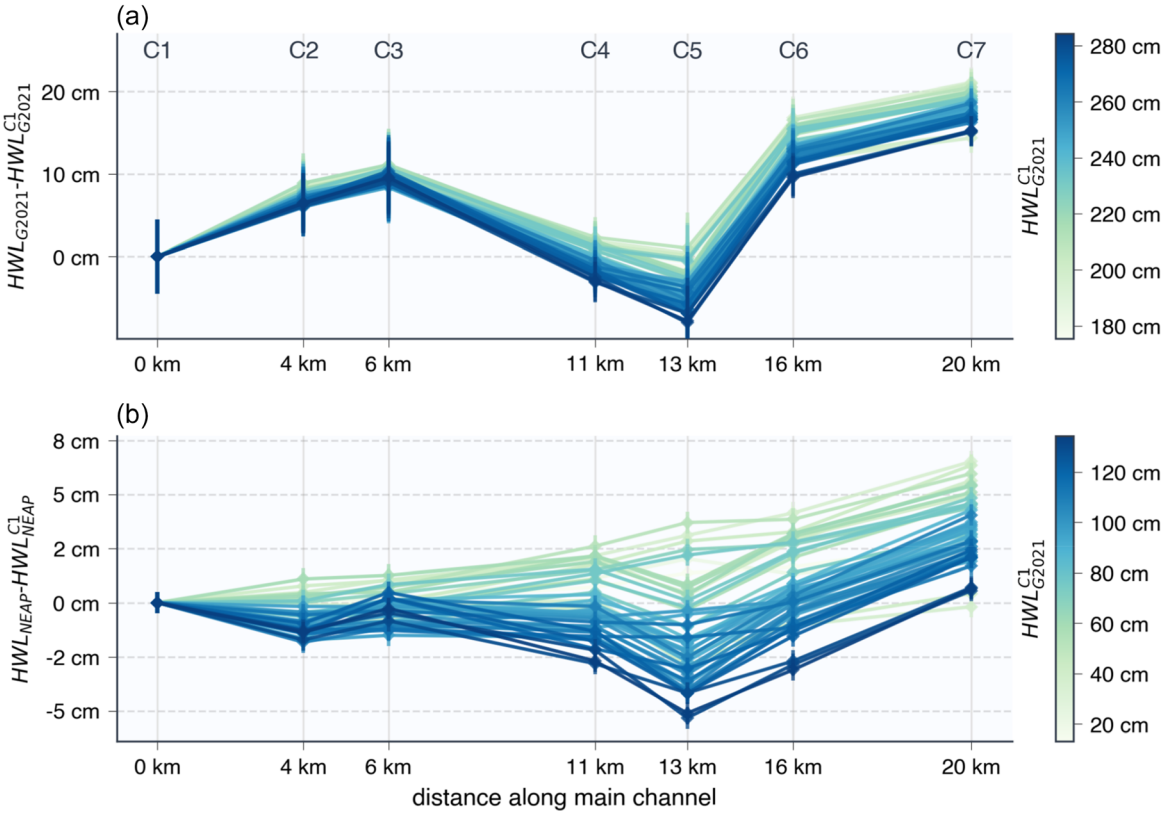

Fig. 5. Difference between high water level along the channel and high water level in C1 for the water level loggers deployed along the main channel (C1–7), plotted against the distance along the main channel starting at C1. Each line represents a tidal wave. Absolute water levels are referenced to GEOID2021 (**a**) and local high water during neap tide (**b**). Each line represents a single high tide between August 28, 2022 and September 20, 2022. Darker blue colors indicate higher incoming water levels at C1 while light green colors indicate lower incoming water levels at C1 ($n = 47$).

Rhizophora's dense network of rigid stilt roots (Fig. 2c) which reaches multiple meters above the mangrove forest floor, in contrast to previous studies on *Avicennia marina*, where pneumatophores are commonly lower than 30 cm high (Fig. 1; Montgomery et al. 2018). This dense network of stilt roots corresponds to a high frontal area, that is the surface area in the vertical plane perpendicular to the water flow (Zhang et al. 2015; Yoshikai et al. 2022). As vegetation-induced drag on water flow is typically considered to increase linearly with the frontal area (Nepf 2012), the high frontal area of *Rizophora*'s dense root network may explain the high attenuation rates compared to previous studies. Calibrated values for C_m range between 1 and 3 (Table 2), which are substantially higher than previously reported values for *Avicennia* sp., which range between 0 and 0.15 (Horstman et al. 2021; Montgomery et al. 2018). Typically, C_d is assumed to be 1, and C_m corresponds with a_v (*see* Eq. 3). Therefore, the high calibrated values for C_m in this study imply a higher a_v for Rhizophora sp. compared to *Avicennia* trees. Lopez-Arias et al. (2024) estimated a_v by counting stilt roots and measuring root diameters in Rhizophora trees at distinctive heights above the forest floor, and reported values ranging from 0.2 to 1.7 within the bottom 50 cm above the sediment. Assuming C_m reflect a_v, our calibrated values for inundations greater than 22 cm (Table 2) fall within the range observed by Lopez-Arias et al. (2024). Reports on the attenuation of short-period wind-driven waves show the strongest attenuation for Rhizophora, compared to *Avicennia* and *Sonneratia*, which is also attributed to Rhizophora's higher frontal area (Quartel et al. 2007; Horstman et al. 2014).

Calibrated values for C_m were larger during tides with lower inundation depths. Root density, and therefore a_v, is typically greater closer to the forest floor (Lopez-Arias et al. 2024; Horstman et al. 2014; Yoshikai et al. 2022). Furthermore, while bottom friction is generally considered negligible compared to vegetation-induced drag (Mazda et al. 1997), we suggest that at lower inundation depths, microtopographic features—such as crab burrows—also contribute substantially to total drag, contributing to the higher calibrated values for C_m at inundation below 27 cm.

While attenuation rates are typically expressed as HWL reduction per kilometer, extrapolating to multiple kilometers should be done with caution as the HWL reduction typically decreases with distance into the forest (Fig. 3) and landscape-scale elements such as channels could strongly affect within-

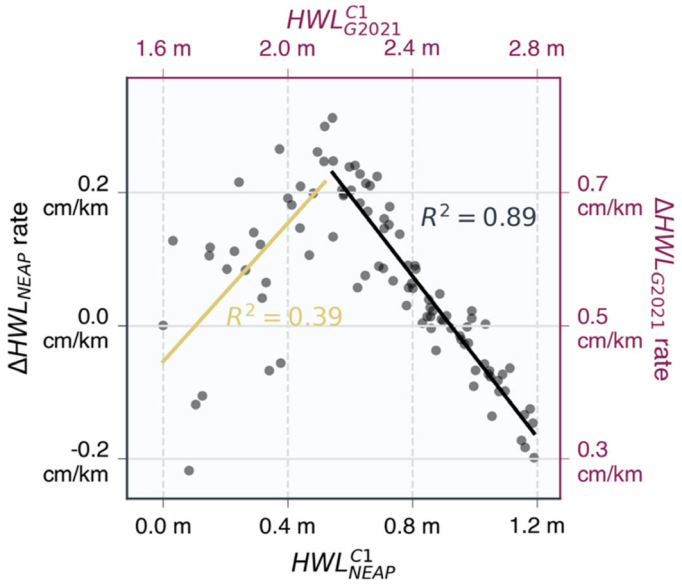

Fig. 6. ΔHWL along the 20-km transect following the channel rates plotted against incoming HWL at C1. ΔHWL rates are calculated as the difference in peak water level for each high tide at logger locations C1 and C6 divided by the water path length in between ($n = 98$). Bottom and left axes are referenced to the neap tide HWL, while the right and top axes are referenced to GEOID2021. For incoming water levels higher than 0.54 m referenced to local neap tide (at which amplification is maximum), there is a negative linear relation ($R^2 = 0.89$, slope $= -0.61$ and intercept $= 0.56$) indicated by the black line. Error bars on the ΔHWL rates are too small to be visible, but note that uncertainty on ΔHWL_{G2021} rates is likely larger than for ΔHWL_{neap} rates.

wetland attenuation rates (Montgomery et al. 2018). We also report exponential attenuation rates (K; *see* Eq. 1 and Table 2), which more accurately capture the modeled high-water levels (HWLs), especially beyond 400 m into the forest (Supporting Information Fig. S7). Higher K values represent stronger attenuation, while lower values indicate weaker attenuation. Unlike linear attenuation rates, the exponential formulation accounts for the decreasing reduction in HWL farther into the forest, helping to avoid overestimation of attenuation at longer distances (e.g., beyond 500 m).

A useful way to interpret K is through the expression $1-e^{-K}$, which gives the proportion of HWL reduction after traveling 1 km into the forest. For example, the highest decay rate observed in this study is 4.12 km^{-1}, corresponding to a 76% reduction in HWL over 1 km (from 40 to 10 cm).

During recorded high water events, inundation did not exceed the height where stilt root density declines. Since vegetation-induced drag decreases above the stilt roots (Maza et al. 2017; Yoshikai et al. 2022), this is relevant. However, in our study area, stilt roots extend several meters above the forest floor (Supporting Information Fig. S2), while extreme sea level events are not expected to exceed 1.2 m (Belliard et al. 2021), so a significant decrease in frontal area is unlikely. Within-wetland attenuation in mangroves has also been shown to decrease for flood events with a longer inundation (Montgomery et al. 2018). However, in macrotidal estuaries such as Churute (~ 4.5 m tidal range), the flood duration would increase in case of extreme sea levels but remain limited to a few hours instead, and as such we do not expect within-wetland attenuation to substantially decrease due to longer flood duration in case of extreme sea level events. The inundation depths in this study are limited to 40 cm and within-wetland attenuation rates do not appear to substantially increase or decrease with incoming water level, although the relatively high uncertainty of the measured rates might hide such a relationship. This lack of a relation contrasts with the findings in *Avicennia*-dominated mangroves from Horstman et al. (2021) and observations in temperate-climate tidal marshes (Stark et al. 2015; Glass et al. 2018), who recorded lower attenuation rates during inundation events with higher inundation height. Both in *Avicennia* mangroves and in marshes, the frontal plant surface area strongly decreases with height already within the first 1 m above the soil surface, which is not the case for *Rhizophora* in our study area (Fig. 2c). The mangrove tree height in our study area ranges between 15 and 30 m, which is common in tropical mangroves closer to the equator (Simard 2019) and as such, we do not consider the canopy of branches and leaves to have an effect on attenuation. However, as stilt root height and density have been shown to increase with canopy height (Mori et al. 2022; Méndez-Alonzo et al. 2015), we also expect a higher frontal area of stilt roots compared to mangroves in the subtropics and temperate regions, further explaining the relatively high attenuation rates presented here. In any case, we expect that *Rhizophora* mangroves with less dense or lower stilt roots would attenuate HWLs less effectively, stressing the need for HWL attenuation observations along the global variety of mangrove types.

Along-channel attenuation

We show that HWLs increase when propagating through a 20-km long channel fringed by mangroves. The ΔHWL_{G2021} rates over the total channel transect range between + 0.7 and + 1.1 cm km^{-1}, but when considering smaller subsections over several kilometers, there is substantial variation, ranging between ΔHWL_{G2021} rates of − 1.3 cm km^{-1} to + 3.4 cm km^{-1} (Fig. 5a). Our results point out that along-channel ΔHWL_{G2021} rates can vary substantially along a channel. Accordingly, to evaluate whether along-channel HWL attenuation is relevant for flood risk mitigation in specific geographic contexts, observations should cover channel lengths of several 10s of km, instead of extrapolating observations over a subsection of a few km to an entire estuary.

$HWLs_{G2021}$ increased upstream for all recorded high tides. Such an upstream increase in HWL is common in funnel-shaped estuaries where the main channel converges upstream, such as the Churute main channel (Van Rijn 2011; Winterwerp et al. 2013; Eslami et al. 2019; Wang et al. 2019).

When water levels exceed 2.1 m (referred to GEOID2021), along-channel ΔHWL rates decrease significantly with increasing water level. We argue that at this water level, water starts to flood and laterally spreads into the fringing mangroves, either through sheet flow or through small intertidal creeks (Horstman et al. 2013). This can lower upstream HWLs and, as such, result in lower ΔHWL rates and thus reduced amplification along the channel, similar to what has been observed in tidal marshes (Stark et al. 2015). The mangrove platform is located around 2.35 m, referred to as GEOID2021, near C1, while ΔHWL rates start to decrease with increasing water level above 2.1 m, referred to as GEOID2021. We hypothesize that the lowest mangrove areas and the small intertidal creeks are located around 2.1 m, but no digital terrain model is available for the study area to confirm this. We highlight that the discussion above is based on a hypothesis, which can be further explored in future research based on the setup of a hydrodynamic model, which includes spatially covering measurements of mangrove topography (for instance, derived from LiDAR measurements).

The effect of the vertical reference has a large effect on the along-channel attenuation rates (Fig. 6) and, as such, when comparing along-channel attenuation rates between locations and studies, the different used reference levels should be considered. Here we present along-channel attenuation rates with two vertical references: a regional geoid (i.e., GEOID2021) and a local neap tide. Spatial variations in mean sea level (over the entire tidal cycle) such as an upstream increase are included in the $HWLs_{G2021}$ but are not in the $HWLs_{NEAP}$ (Supporting Information Fig. S8). Hence, attenuation rates based on $HWLs_{G2021}$ include these spatial variations together with spatial variations in tidal amplitude. Attenuation rates calculated with $HWLs_{NEAP}$ do not include spatial variations in mean sea level but only the evolution of the tidal amplitude along the transect. The latter is better suited to assess the effect of mangroves, which affect the tidal amplitude but cannot vertically shift the entire tidal cycle. As the loggers were installed between high and low water, we did not record full tidal signals along the main channel.

While our observations only include HWLs during an astronomical spring-neap cycle, the increase in along-channel attenuation with increasing incoming HWLs implies that along-channel attenuation can be lower in case of extreme sea level events. In the Churute area, such extreme sea level events have resulted in incoming water levels 60 cm higher than astronomical spring tide (Belliard et al. 2021; Pelckmans et al. 2024). Extrapolating the linear relation shown in Fig. 6, HWLs would be attenuated at a rate of $-0.9\ \mathrm{cm\ km^{-1}}$. However, whether along-channel ΔHWL can be linearly extrapolated remains very uncertain, and to confirm our hypothesis, we the use of models which explicitly include the vertical variation in mangrove drag to confirm this stronger attenuation in case of extreme sea level.

The observed along-channel ΔHWL_{G2021} rates are positive, indicating HWL amplification, while within-wetland ΔHWL rates are negative, indicating HWL attenuation (Figs. 4, 6). Noteworthy, we measured the strongest within-wetland attenuation ever recorded while measuring along-channel amplification (positive ΔHWL_{G2021} rates). In addition to the important role of the funnel-shaped channel geometry, this may be potentially explained as the high frontal area of *Rhizophora* and consequently high drag slowing down the lateral flow from the channels into the mangroves, and, as such, the high drag of *Rhizophora*'s stilt roots would have a negative effect on along-channel attenuation. In our study, we found along-channel amplification, while Krauss et al. (2007) and Montgomery et al. (2018) found along-channel attenuation. This may suggest that there is a trade-off between within-wetland and along-channel attenuation, determined by the vegetation-induced drag of the mangroves, where a higher frontal area of mangrove roots leads to stronger within-wetland attenuation but weaker along-channel attenuation and vice versa. Future modeling studies could confirm and elucidate this potential trade-off by simulating within-wetland and along-channel attenuation under varying vegetation-induced drag scenarios.

Furthermore, our findings imply that mangrove platform elevation is an important driver of along-channel attenuation, which has also been shown based on hydrodynamic modeling studies for salt marshes (Smolders et al. 2015; Stark et al. 2016) or a large tropical delta with mangroves (Pelckmans et al. 2023). Nevertheless, mangrove platform topography is rarely mapped due to the dense canopy prohibiting GPS surveys or remote sensing (Gijsman et al. 2021). Here we show that trigonometric leveling using a total station can be used to survey mangrove topography along a transect. Moreover, state-of-the-art remote sensing techniques such as high-density LiDAR may potentially further allow topographic surveys of sub-canopy mangrove topography. While previous studies have elaborated on the vegetation-induced drag of mangroves (Ohira et al. 2013; Chen et al. 2021; Chang et al. 2022; Yoshikai et al. 2022), we believe that mangrove platform topography is still an understudied key factor in HWL reduction by mangroves, which is essential to maximize the flood risk mitigation capacity of mangroves.

Implications for nature-based flood risk management

Our observations stress the potential for mangroves to attenuate extreme HWL events, especially when areas at risk are separated from the coast or from estuarine channels by continuous mangroves. When areas at risk are located upstream along an estuarine or deltaic channel, fringing mangroves can limit HWL amplification and reduce upstream flood risks, but at rates much weaker than within-wetland attenuation. With higher incoming HWLs, along-channel attenuation is expected to become stronger. In any case,

effective flood risk mitigation requires substantially long channel sections fringed by mangroves.

While previous studies have mostly focused on *Avicennia marina* or subtropical mangrove-marsh mixtures, we present observations in tropical Rhizophora mangroves, showing the strongest attenuation rates recorded in mangroves so far. A global species distribution study has identified *Rhizophora* mangroves to be the most common mangrove species among mangroves that are most exposed to tides and waves (Twomey and Lovelock 2024). We suggest future studies that assess flood damage reduction by mangroves to consider the appropriate attenuation rates for the dominant species, including the strong attenuation rates presented in this study for *Rhizophora*. More importantly, local, regional, and global studies that quantify the prevented financial and human loss by mangrove flood risk mitigation (e.g., Menéndez 2020; Van Coppenolle 2018) should not simply extrapolate within-wetland attenuation rates to entire mangrove forests or assume continuous mangroves with uniform bed roughness but instead include channel networks along which attenuation is substantially lower.

Author Contributions

Ignace Pelckmans: conceptualization, formal analysis, funding acquisition, project administration, investigation, methodology, visualization, writing—original draft preparation, writing—review and editing. Ben Vermeulen: investigation. John Alex Ramos-Veliz: investigation. Andrea Mishell Rosado-Moncayo: investigation, project administration. Jean-Philippe Belliard: conceptualization, supervision, writing—review and editing. Olivier Gourgue: conceptualization, supervision, writing—review and editing. Cornelis Slobbe: formal analysis, writing—review and editing. Luis E. Dominguez-Granda: conceptualization, funding acquisition, project administration, investigation, supervision, writing—review and editing. Stijn Temmerman: conceptualization, supervision, investigation, writing—review and editing.

Acknowledgments

The study was locally supported in the context of the VLIR-UOS Ecuador Biodiversity Network project. The field campaign was supported by the facilities provided by park rangers at the Manglares Churute Ecological Reserve from the Ministry of Environment, Water and Ecological Transition of Ecuador. Ignace Pelckmans has been supported by a PhD fellowship for fundamental research funded by the Research Foundation Flanders (FWO, Belgium, grant no. 11E0723N), Jean-Philippe Belliard has been supported by FED-tWIN ABioGrad, and Olivier Gourgue has been supported by the European Union's Horizon 2020 research and innovation program under the Marie-Sklodowska-Curie grant agreement no. 798222.

Conflicts of Interest

None declared.

References

Belliard, J.-P., L. E. Dominguez-Granda, J. A. Ramos-Veliz, et al. 2021. "El Niño Driven Extreme Sea Levels in an Eastern Pacific Tropical River Delta: Landward Amplification and Shift from Oceanic to Fluvial Forcing." *Global and Planetary Change* 203: 103529. https://doi.org/10.1016/j.gloplacha.2021.103529.

Chang, C., N. Mori, N. Tsuruta, K. Suzuki, and H. Yanagisawa. 2022. "An Experimental Study of Mangrove-Induced Resistance on Water Waves Considering the Impacts of Typical Rhizophora Roots." *Journal of Geophysical Research: Oceans* 127: e2022JC018653. https://doi.org/10.1029/2022jc018653.

Chen, L. 2016. "Pneumatophores." In Encyclopedia of Earth Sciences Series, Edited by M.J. Kennish, 494. Springer. https://doi.org/10.1007/978-94-017-8801-4_282.

Chen, Q., Y. Li, D. M. Kelly, K. Zhang, B. Zachry, and J. Rhome. 2021. "Improved Modeling of the Role of Mangroves in Storm Surge Attenuation." *Estuarine, Coastal and Shelf Science* 260: 107515. https://doi.org/10.1016/j.ecss.2021.107515.

Dahdouh-Guebas, F., L. P. Jayatissa, D. D. Nitto, J. O. Bosire, D. L. Seen, and N. Koedam. 2005. "How Effective Were Mangroves as a Defence against the Recent Tsunami?" *Current Biology* 15: R443–R447. https://doi.org/10.1016/j.cub.2005.06.008.

Das, S., and J. R. Vincent. 2009. "Mangroves Protected Villages and Reduced Death Toll during Indian Super Cyclone." *Proceedings of the National Academy of Sciences of the United States of America* 106: 7357–7360. https://doi.org/10.1073/pnas.0810440106.

de Matos, A. C. O. C., D. Blitzkow, G. d. N. Guimarães, and V. C. Silva. 2021. The South American Gravimetric Geoid: GEOID2021. V. 1.0. GFZ Data Services. https://doi.org/10.5880/isg.2021.006.

Deb, M., and C. M. Ferreira. 2017. "Potential Impacts of the Sunderban Mangrove Degradation on Future Coastal Flooding in Bangladesh." *Journal of Hydro-Environment Research* 17: 30–46. https://doi.org/10.1016/j.jher.2016.11.005.

del Valle, A., M. Eriksson, O. A. Ishizawa, and J. J. Miranda. 2020. "Mangroves Protect Coastal Economic Activity from Hurricanes." *Proceedings of the National Academy of Sciences of the United States of America* 117: 265–270. https://doi.org/10.1073/pnas.1911617116.

Eslami, S., P. Hoekstra, N. N. Trung, et al. 2019. "Tidal Amplification and Salt Intrusion in the Mekong Delta Driven by Anthropogenic Sediment Starvation." *Scientific Reports* 9: 18746. https://doi.org/10.1038/s41598-019-55018-9.

Fox-Kemper, B., H. T. Hewitt, C. Xiao, et al. 2021. "Ocean, Cryosphere and Sea Level Change." In Climate Change 2021—The Physical Science Basis, edited by V. Masson-Delmotte, P. Zhai, A. Pirani, et al., Cambridge University Press: 1211–1362. https://doi.org/10.1017/9781009157896.011.

Gijsman, R., E. M. Horstman, D. van der Wal, D. A. Friess, A. Swales, and K. M. Wijnberg. 2021. "Nature-Based Engineering: A Review on Reducing Coastal Flood Risk with Mangroves." *Frontiers in Marine Science* 8: 702412. https://doi.org/10.3389/fmars.2021.702412.

Glass, E. M., J. L. Garzon, S. Lawler, E. Paquier, and C. M. Ferreira. 2018. "Potential of Marshes to Attenuate Storm Surge Water Level in the Chesapeake Bay." *Limnology and Oceanography* 63: 951–967. https://doi.org/10.1002/lno.10682.

Glavovic, B. C., R. Dawson, W. Chow, et al. 2022. Cross-Chapter Paper 2: Cities and Settlements by the Sea, edited by H. O. Pörtner, D. C. Roberts, M. Tignor, et al., Cambridge: Cambridge University Press: 2163–2194. https://doi.org/10.1017/9781009325844.019.2163.

Horstman, E. M., K. R. Bryan, and J. C. Mullarney. 2021. "Drag Variations, Tidal Asymmetry and Tidal Range Changes in a Mangrove Creek System." *Earth Surface Processes and Landforms* 46: 1828–1846. https://doi.org/10.1002/esp.5124.

Horstman, E. M., C. M. Dohmen-Janssen, and S. J. M. H. Hulscher. 2013. "Flow Routing in Mangrove Forests: A Field Study in Trang Province, Thailand." *Continental Shelf Research* 71: 52–67. https://doi.org/10.1016/j.csr.2013.10.002.

Horstman, E. M., C. M. Dohmen-Janssen, P. M. F. Narra, N. J. F. van den Berg, M. Siemerink, and S. J. M. H. Hulscher. 2014. "Wave Attenuation in Mangroves: A Quantitative Approach to Field Observations." *Coastal Engineering* 94: 47–62. https://doi.org/10.1016/j.coastaleng.2014.08.005.

INAMHI. 2019. "Official INAMHI Website."

Kathiresan, K., and N. Rajendran. 2005. "Coastal Mangrove Forests Mitigated Tsunami." *Estuarine, Coastal and Shelf Science* 65: 601–606. https://doi.org/10.1016/j.ecss.2005.06.022.

Klees, R., and D. C. Slobbe. 2023. "Variance–Covariance Analysis of Two High-Resolution Regional Least-Squares Quasi-Geoid Models." *Journal of Geodesy* 97, no. 8: 80. https://doi.org/10.1007/s00190-023-01772-8.

Kobashi, D., and Y. Mazda. 2005. "Tidal Flow in Riverine-Type Mangroves." *Wetlands Ecology and Management* 13, no. 6: 615–619. https://doi.org/10.1007/s11273-004-3481-4.

Krauss, K. W., J. A. Allen, and D. R. Cahoon. 2003. "Differential Rates of Vertical Accretion and Elevation Change among Aerial Root Types in Micronesian Mangrove Forests." *Estuarine, Coastal and Shelf Science* 56: 251–259. https://doi.org/10.1016/s0272-7714(02)00184-1.

Krauss, K. W., T. W. Doyle, T. J. Doyle, et al. 2009. "Water Level Observations in Mangrove Swamps during Two Hurricanes in Florida." *Wetlands* 29: 142–149. https://doi.org/10.1672/07-232.1.

Lopez-Arias, F., M. Maza, F. Calleja, G. Govaere, and J. L. Lara. 2024. "Integrated Drag Coefficient Formula for Estimating the Wave Attenuation Capacity of *Rhizophora sp*. Mangrove Forests." *Frontiers in Marine Science* 11: 1383368. https://doi.org/10.3389/fmars.2024.1383368.

Maza, M., K. Adler, D. Ramos, A. M. Garcia, and H. Nepf. 2017. "Velocity and Drag Evolution From the Leading Edge of a Model Mangrove Forest." *Journal of Geophysical Research: Oceans* 122: 9144–9159. https://doi.org/10.1002/2017jc012945.

Mazda, Y., E. Wolanski, B. King, A. Sase, D. Ohtsuka, and M. Magi. 1997. "Drag Force Due to Vegetation in Mangrove Swamps." *Mangroves and Salt Marshes* 1: 193–199. https://doi.org/10.1023/a:1009949411068.

Menéndez, P., I. J. Losada, S. Torres-Ortega, S. Narayan, and M. W. Beck. 2020. "The Global Flood Protection Benefits of Mangroves." *Scientific Reports* 10, no. 1: 4404. https://doi.org/10.1038/s41598-020-61136-6.

Montgomery, J., K. Bryan, E. Horstman, and J. Mullarney. 2018. "Attenuation of Tides and Surges by Mangroves: Contrasting Case Studies from New Zealand." *Water (Basel)* 10: 1119. https://doi.org/10.3390/w10091119.

Mori, N., C.-W. Chang, T. Inoue, et al. 2022. "Parameterization of Mangrove Root Structure of *Rhizophora stylosa* in Coastal Hydrodynamic Model." *Frontiers in Built Environment* 7: 782219. https://doi.org/10.3389/fbuil.2021.782219.

Méndez-Alonzo, R., C. Moctezuma, V. R. Ordoñez, G. Angeles, A. J. Martínez, and J. López-Portillo. 2015. "Root Biomechanics in Rhizophora Mangle: Anatomy, Morphology and Ecology of Mangrove's Flying Buttresses." *Annals of Botany* 115, no. 5: 833–840. https://doi.org/10.1093/aob/mcv002.

Nepf, H. M. 2012. "Flow and Transport in Regions with Aquatic Vegetation." *Annual Review of Fluid Mechanics* 44: 123–142. https://doi.org/10.1146/annurev-fluid-120710-101048.

Ohira, W., K. Honda, M. Nagai, and A. Ratanasuwan. 2013. "Mangrove Stilt Root Morphology Modeling for Estimating Hydraulic Drag in Tsunami Inundation Simulation." *Trees* 27: 141–148. https://doi.org/10.1007/s00468-012-0782-8.

Ong, J. E., W. K. Gong, and C. H. Wong. 2004. "Allometry and Partitioning of the Mangrove, *Rhizophora apiculata*." *Forest Ecology and Management* 188: 395–408. https://doi.org/10.1016/j.foreco.2003.08.002.

Pelckmans, I., J.-P. Belliard, L. E. Dominguez-Granda, C. Slobbe, S. Temmerman, and O. Gourgue. 2023. "Mangrove Ecosystem Properties Regulate High Water Levels in a River Delta." *Natural Hazards and Earth System Sciences* 23: 3169–3183. https://doi.org/10.5194/nhess-23-3169-2023.

Pelckmans, I., J.-P. Belliard, O. Gourgue, L. E. Dominguez-Granda, and S. Temmerman. 2024. "Mangroves as Nature-Based Mitigation for ENSO-Driven Compound Flood Risks in a Large River Delta." *Hydrology and Earth System Sciences*

28, no. 6: 1463–1476. https://doi.org/10.5194/hess-28-1463-2024.

Pil, M. W., M. R. T. Boeger, V. C. Muschner, M. R. Pie, A. Ostrensky, and W. A. Boeger. 2011. "Postglacial North–South Expansion of Populations of *Rhizophora mangle* (Rhizophoraceae) along the Brazilian Coast Revealed by Microsatellite Analysis." *American Journal of Botany* 98: 1031–1039. https://doi.org/10.3732/ajb.1000392.

Quartel, S., A. Kroon, P. G. E. F. Augustinus, P. V. Santen, and N. H. Tri. 2007. "Wave Attenuation in Coastal Mangroves in the Red River Delta, Vietnam." *Journal of Asian Earth Sciences* 29: 576–584. https://doi.org/10.1016/j.jseaes.2006.05.008.

Record, S., N. D. Charney, R. M. Zakaria, and A. M. Ellison. 2013. "Projecting Global Mangrove Species and Community Distributions under Climate Change." *Ecosphere* 4: 1–23. https://doi.org/10.1890/es12-00296.1.

Sandoval-Castro, E., R. Muñiz-Salazar, L. M. Enríquez-Paredes, et al. 2012. "Genetic Population Structure of Red Mangrove (*Rhizophora mangle* L.) along the Northwestern Coast of Mexico." *Aquatic Botany* 99: 20–26. https://doi.org/10.1016/j.aquabot.2012.01.002.

Simard, M., L. Fatoyinbo, C. Smetanka, et al. 2019. "Mangrove Canopy Height Globally Related to Precipitation, Temperature and Cyclone Frequency." *Nature Geoscience* 12, no. 1: 40–45. https://doi.org/10.1038/s41561-018-0279-1.

Slobbe, D. C., M. Verlaan, R. Klees, and H. Gerritsen. 2013. "Obtaining Instantaneous Water Levels Relative to a Geoid with a 2D Storm Surge Model." *Continental Shelf Research* 52: 172–189. https://doi.org/10.1016/j.csr.2012.10.002.

Smolders, S., Y. Plancke, S. Ides, P. Meire, and S. Temmerman. 2015. "Role of Intertidal Wetlands for Tidal and Storm Tide Attenuation along a Confined Estuary: A Model Study." *Natural Hazards and Earth System Sciences* 15: 1659–1675. https://doi.org/10.5194/nhess-15-1659-2015.

Stark, J., T. Oyen, P. Meire, and S. Temmerman. 2015. "Observations of Tidal and Storm Surge Attenuation in a Large Tidal Marsh." *Limnology and Oceanography* 60: 1371–1381. https://doi.org/10.1002/lno.10104.

Stark, J., Y. Plancke, S. Ides, P. Meire, and S. Temmerman. 2016. "Coastal Flood Protection by a Combined Nature-Based and Engineering Approach: Modeling the Effects of Marsh Geometry and Surrounding Dikes." *Estuarine, Coastal and Shelf Science* 175: 34–45. https://doi.org/10.1016/j.ecss.2016.03.027.

Tebaldi, C., R. Ranasinghe, M. Vousdoukas, et al. 2021. "Extreme Sea Levels at Different Global Warming Levels." *Nature Climate Change* 11: 746–751. https://doi.org/10.1038/s41558-021-01127-1.

Temmerman, S., E. M. Horstman, K. W. Krauss, J. C. Mullarney, I. Pelckmans, and K. Schoutens. 2023. "Marshes and Mangroves as Nature-Based Coastal Storm Buffers." *Annual Review of Marine Science* 15: 95–118. https://doi.org/10.1146/annurev-marine-040422-092951.

Twomey, A., and C. Lovelock. 2024. "Global Spatial Dataset of Mangrove Genus Distribution in Seaward and Riverine Margins." *Scientific Data* 11: 306. https://doi.org/10.1038/s41597-024-03134-1.

Van Coppenolle, R., C. Schwarz, and S. Temmerman. 2018. "Contribution of Mangroves and Salt Marshes to Nature-Based Mitigation of Coastal Flood Risks in Major Deltas of the World." *Estuaries and Coasts* 41, no. 6: 1699–1711. https://doi.org/10.1007/s12237-018-0394-7.

Van Rijn, L. C. 2011. "Analytical and Numerical Analysis of Tides and Salinities in Estuaries; Part I: Tidal Wave Propagation in Convergent Estuaries." *Ocean Dynamics* 61: 1719–1741. https://doi.org/10.1007/s10236-011-0453-0.

Wang, Z. B., W. Vandenbruwaene, M. Taal, and H. Winterwerp. 2019. "Amplification and Deformation of Tidal Wave in the Upper Scheldt Estuary." *Ocean Dynamics* 69: 829–839. https://doi.org/10.1007/s10236-019-01281-3.

Winterwerp, J. C., Z. B. Wang, A. van Braeckel, G. van Holland, and F. Kösters. 2013. "Man-Induced Regime Shifts in Small Estuaries—II: A Comparison of Rivers." *Ocean Dynamics* 63: 1293–1306. https://doi.org/10.1007/s10236-013-0663-8.

Yoshikai, M., T. Nakamura, D. M. Bautista, et al. 2022. "Field Measurement and Prediction of Drag in a Planted Rhizophora Mangrove Forest." *Journal of Geophysical Research: Oceans* 127: e2021JC018320. https://doi.org/10.1029/2021jc018320.

Zhang, K., H. Liu, Y. Li, et al. 2012. "The Role of Mangroves in Attenuating Storm Surges." *Estuarine, Coastal and Shelf Science* 102: 11–23. https://doi.org/10.1016/j.ecss.2012.02.021.

Zhang, W., Z.-M. Ge, S.-H. Li, et al. 2022. "The Role of Seasonal Vegetation Properties in Determining the Wave Attenuation Capacity of Coastal Marshes: Implications for Building Natural Defenses." *Ecological Engineering* 175: 106494. https://doi.org/10.1016/j.ecoleng.2021.106494.

Zhang, X., V. P. Chua, and H.-F. Cheong. 2015. "Hydrodynamics in Mangrove Prop Roots and their Physical Properties." *Journal of Hydro-Environment Research* 9: 281–294. https://doi.org/10.1016/j.jher.2014.07.010.

Supporting Information

Additional Supporting Information may be found in the online version of this article.

Submitted 30 July 2024
Revised 27 May 2025
Accepted 29 June 2025